

## MICROBEAM X-RAY DIFFRACTION PATTERNS OF THE SERPENTINE MINERALS

F. J. WICKS<sup>1</sup> AND J. ZUSSMAN<sup>2</sup>

Department of Geology & Mineralogy, Oxford University, Oxford, England

### ABSTRACT

The microbeam x-ray diffraction camera has been used to study the serpentine minerals *in-situ* in thin section. Distinctive diffraction patterns of chrysotile  $2M_{c1}$ , chrysotile  $2Or_{c1}$ , parachrysotile, lizardite 1-layer, 2-layer and 6-layer polytypes, and antigorite have been recorded. The cylindrical structure of chrysotile with its disorder around the x-axis (fiber-axis) produces "rotation type" diffraction patterns. Parachrysotile with  $\gamma$  parallel to the fiber-axis, was recorded only in association with chrysotile  $2M_{c1}$  or chrysotile  $2Or_{c1}$ . Lizardite 1T produces a variety of diffraction patterns depending upon which crystallographic axis is parallel to the x-ray microbeam. Lizardite plates occur in two types of orientation; those in mesh and hourglass textures, after olivine and other silicates, tend to have their z-axes parallel, whereas those occurring as orthopyroxene-bastites tend to have their x-axes parallel. Antigorite produces near-"rotation type" diffraction patterns which indicate that the antigorite blades tend to be fairly strongly oriented with their y-axes parallel, but with partial disorientation around the average y-axis position.

In spite of the fibrous appearance of most of the serpentine minerals in thin section, the microbeam diffraction patterns indicate that only chrysotile is truly fibrous, and that lizardite and antigorite occur as plates or laths. The optical classification of apparent serpentine fibers has limited mineralogical meaning. Apparently-fibrous  $\alpha$ -serpentine is often lizardite, but  $\gamma$ -serpentine may be chrysotile, lizardite, or antigorite. Serpophite (isotropic in thin section) may be chrysotile, lizardite, or a mixture of the two.

### INTRODUCTION

The classification of the serpentine minerals has been based primarily on x-ray diffraction studies of single crystals and fiber bundles. The serpentine minerals responsible for the characteristic textures of serpentinized ultramafic rocks are too fine-grained to be studied by single-crystal methods and thus have been studied

by x-ray powder-diffraction techniques. However, crushing the samples to a fine powder makes it impossible to determine the relationships of the various serpentine minerals within the textures. Since the textural units vary in size from 40 to 400 microns, the microbeam (50 micron diameter) x-ray camera can be used to identify minerals *in situ* in thin section so that the classification based on the single-crystal studies can be applied directly to the fine-grained minerals.

In a simple microbeam camera such as the one used in this study the part of the thin section containing the area to be x-rayed is fixed in a plane perpendicular to the x-ray microbeam. A single crystal of 50 microns diameter, or larger, would probably be in an arbitrary orientation with respect to the plane of the thin section and would thus produce a diffraction pattern that would be difficult to interpret. However, in serpentine minerals the grain size is fine enough to ensure that many crystallites are present within the 50 micron diameter area irradiated, and there is enough disorientation between, or distortion within, the crystallites to produce diffraction patterns intermediate between single-crystal patterns and powder diffraction patterns. These factors combine to produce microbeam diffraction patterns that can be interpreted in a fairly simple manner.

This paper discusses the different types of microbeam x-ray diffraction patterns produced by the various serpentine minerals, and relates the optical properties to the crystallographic axes of the serpentine minerals. The classification of the serpentine minerals upon which this discussion is based is essentially that of Whittaker & Zussman (1956) modified by Wicks & Whittaker (1975).

### EXPERIMENTAL PROCEDURES

The Norelco microbeam x-ray diffraction camera equipped with a standard 50 micron diameter Pb-glass collimator was used in this study. The camera was designed by Chesley (1947) for application to problems in metallurgy, and the commercial model has been de-

<sup>1</sup>Present address: Mineralogy Department, Royal Ontario Museum, Toronto, Canada.

<sup>2</sup>Present address: Department of Geology, The University, Manchester, England.

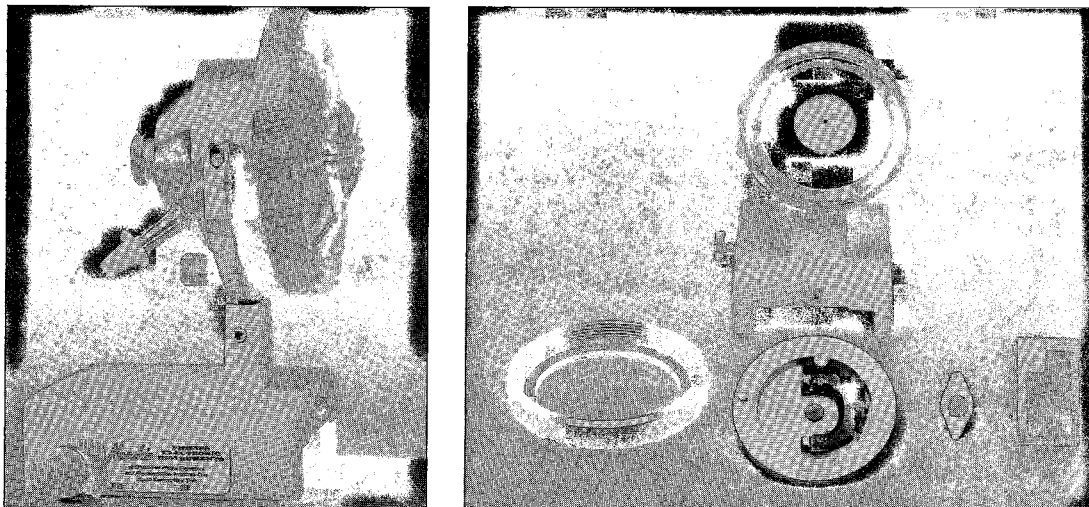


FIG. 1. Microbeam *x*-ray camera assembled. Bottom edge of stand is 8.4 cm. The back of the camera (left) contains the direct beam trap and a tube for attaching a vacuum pump. The collimator is in the center of the front of the camera.

FIG. 2. Microbeam *x*-ray camera components, left to right. 1) knurled ring that holds the two parts of the camera together, 2) front of camera containing the specimen holder and the collimator (center), 3) fragment of thin section glued to Mylar film on an aluminum frame, and 4) thin section with fragment removed. The back of the camera containing the film holder with film.

scribed in detail by Bergmann (1959). The camera is composed of two parts (Figs. 1 and 2). The front contains the Pb-glass collimator and a specimen holder that pivots about a fixed point and traverses in one direction. The back of the camera contains a flat-plate film holder, a fluorescent screen and Pb-glass direct-beam stop. The holder takes a  $35 \times 40$  mm film and, with a film to sample distance of 15 mm, records a circular pattern up to  $45^\circ$  of  $2\theta$  with Cu radiation. When the two parts are assembled, the camera rests in a cradle stand, the base of which fits on the standard Phillips powder camera track. The procedure for aligning the microbeam camera with the *x*-ray source has been given in detail by Bergmann (1959). Exposures with nickel-filtered copper radiation at settings of 36kV and 20 ma from both standard (18 hrs.) and fine-focus (10 hrs.) *x*-ray tubes were used in this study.

The techniques for sample preparation were similar to those described by Carrigy, Mellon and Potheary (1964). Thin sections were prepared by normal procedures, but were left uncovered. Fragile samples were left slightly thicker than normal. When textures suitable for *x*-ray diffraction study were observed under the petrographic microscope the appropriate area of the thin section was marked off. The thin section was then heated to soften the Lakeside ad-

hesive and the area containing the selected texture, generally smaller than  $10 \times 10$  mm, was cut out of the thin section and washed with methanol. The sample was then mounted with diluted Durofix on a Mylar film that had previously been attached, with diluted Durofix, to a thin aluminium frame shaped to fit the adjustable sample holder of the camera (Fig. 2). The Mylar film gives a diffuse diffraction ring of approximately  $d = 5.8\text{\AA}$  but this does not interfere with the serpentine diffraction patterns.

Once the Durofix had hardened, the aluminium frame containing the sample was placed under the petrographic microscope and the area to be *x*-rayed was sketched. The aluminium frame was then mounted in the sample holder and the entire front part of the camera was placed on the stage of a petrographic microscope. The light source of the microscope provided illumination through the 50 micron Pb-glass collimator, and the particular feature to be *x*-rayed was moved over the collimator by pivoting and translating the sample holder. In some cases the Pb-glass collimator had to be removed before the selected feature could be located and positioned approximately at the center of the collimator opening. Then the collimator was replaced and the final adjustment was made. The area to be exposed to the *x*-rays was then marked on the sketch of the texture.

Finally a film was placed in the back of the camera which was then assembled and mounted on the camera track. Once the camera had been aligned as outlined by Bergmann (1959), only a slight adjustment was necessary to obtain the proper passage of the beam through the camera. As long as the camera was handled gently, there was no problem of the sample holder moving out of alignment.

The standard diffraction patterns of the serpentine minerals were drafted to scale on acetate sheets for rapid identification. If necessary, the films can be measured accurately with a travelling microscope, but usually an internal standard such as gold foil (Carrigy & Mellon 1964) is required. Internal standards were not used in this study since identification, and not the measurement of  $d$ -spacings, was the main object. However, in several exposures weak reflections from other minerals were found associated with the serpentine reflections. In these cases the spacings of the serpentine reflections were determined with a 114.6 mm Debye-Scherrer camera and then were used as an internal standard on the microbeam diffraction patterns. The accessory minerals will be the subject of a separate publication.

#### SAMPLES

Fifty-six thin sections from 31 ultramafic bodies were examined and more than 250 x-ray microbeam photographs from a wide variety of textures were recorded. The results of this study have been recorded by Wicks (1969). The present paper is restricted to a discussion of the

microbeam x-ray diffraction patterns of the various serpentine minerals and the relationship of the optical properties to the crystallographic axes. The detailed mineralogy of the serpentine textures is the subject of a separate paper (Wicks & Whittaker, in preparation).

#### MICROBEAM DIFFRACTION PATTERNS

Each of the serpentine minerals, chrysotile, lizardite and antigorite, produces distinctive diffraction patterns that have some of the features of rotation-type diffraction patterns, even though the specimen is stationary in the microbeam camera. Most of the diffraction patterns display the effects of one or both of two types of disorientation: (1) the fiber axis or appropriate crystallographic axis may not be perpendicular to the x-ray beam, or (2) the crystals or fibers may not be in a perfectly parallel orientation with respect to one another.

The effect of the first type of disorientation is illustrated in Figure 3. The fiber axis is inclined towards the lower half and away from the upper half of the film and the lower reflections are drawn together while the upper reflections are spread apart.

The effect of the second type of disorientation is illustrated in Figure 4. As the degree of disorientation of the crystals or fibers about an axis increases, the reflections are increasingly spread out into arcs that follow along Debye-Scherrer rings. In the extreme case where all crystals are randomly oriented, all reflections form complete Debye-Scherrer rings.

The various diffraction patterns are described

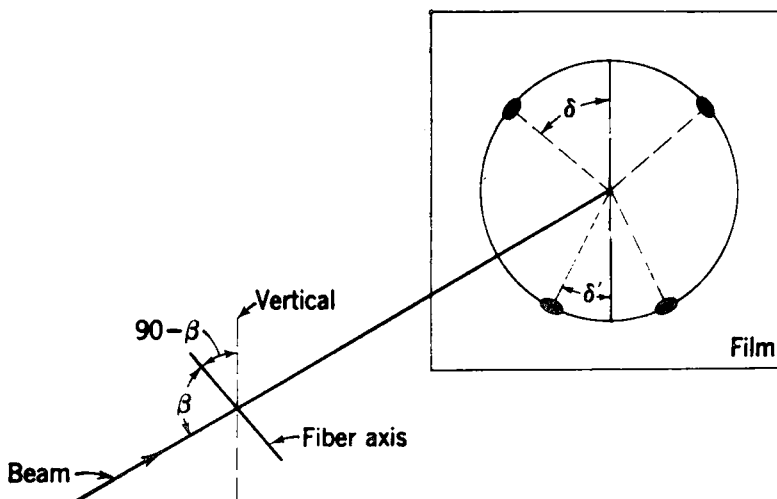


FIG. 3. The effect of tilting the fiber axis on the positions of intensity maxima (from Klug & Alexander 1954).

in terms of diagrammatic idealized models (Fig. 5). The actual recorded diffraction patterns (Fig. 6) rarely possess the perfection of the models.

### Chrysotile

The cylindrical structure of chrysotile produces disorder around the  $x$ -axis (the fiber axis) so that no change is produced in the diffraction pattern, when a specimen is turned about the  $x$ -axis to a new position. The diffraction pattern of chrysotile  $2M_{c1}$  with the  $x$ -axis normal to the microbeam is illustrated diagrammatically in Figure 5a, and chrysotile  $2Or_{c1}$  in Figure 5b. (The chrysotile polytype nomenclature used here was developed by Wicks & Whittaker (1975);  $2M$  = a 2-layer monoclinic unit cell,  $2Or$  = a 2-layer orthorhombic unit cell,  $c$  = cylindrical, and 1 = polytype number). The microbeam diffraction patterns are similar to a normal fiber diffraction pattern recorded with an oscillation, or a rotation camera except that the layer lines are slightly hyperbolic, because they are recorded on a flat film. In chrysotile  $2M_{c1}$  and chrysotile  $2Or_{c1}$  the zero-layer lines are composed of  $00l$  and  $020$  reflections and the first and third-order lines of  $1k0$  and  $3k0$  reflections with diffuse streaks sweeping away to higher angles (Fig. 6a). In chrysotile  $2M_{c1}$ ,  $\beta$  is  $93^\circ 16'$  (Whittaker 1956a) and the second-layer line is made up of  $202$ ,  $202$ ,  $203$ ,  $204$ , and  $204$  reflections. In chrysotile  $2Or_{c1}$ ,  $\beta$  is  $90^\circ$  (Whittaker 1956b) and the pairs of  $20\bar{l}$  and  $20l$  reflections coincide at points midway between the position of the pairs of chrysotile  $2M_{c1}$  reflections. In Figure 6b reflections from both chry-

sotile  $2M_{c1}$  and  $2Or_{c1}$  are present. The  $20l$  reflections of the chrysotile  $2M_{c1}$  and  $2Or_{c1}$  examined, indicate that both have a 2-layer unit cell (Whittaker 1953). No 1-layer chrysotile  $1M_{c1}$  or  $1M_{c2}$  was encountered (Zvyagin 1967; Wicks & Whittaker 1975).

Tilting of the  $x$ -axis of chrysotile  $2M_{c1}$  and chrysotile  $2Or_{c1}$  so that it is no longer normal to the  $x$ -ray microbeam, draws together the  $20l$  and  $1k0$  reflections on one side of the film, and spreads them apart on the opposite side of the film, as illustrated diagrammatically in Figure 3. A tilt of approximately  $17^\circ$  can bring the  $200$  plane into diffraction position on one side of the film (Fig. 6c), but extreme tilting can drastically alter the diffraction pattern by producing Debye-Scherrer arcs and rings (Fig. 6d).

The shape of the reflections may vary considerably. Sharp diffraction spots or short Debye-Scherrer arcs of less than  $10^\circ$ , associated with very weak complete or incomplete Debye-Scherrer rings (Fig. 6a), have been recorded on diffraction patterns from parallel fibers of chrysotile asbestos. Not all the microbeam diffraction patterns indicate such good parallel orientation. Debye-Scherrer arcs of  $20^\circ$  to  $60^\circ$  (measured on  $004$ ) develop when the fibers within the irradiated area lie in two or more well-defined orientations (Fig. 6b). Zones of strong intensity develop where the layer lines and the Debye-Scherrer arcs intersect, and the arcs end abruptly with a sharp drop in intensity. However, a complete, weakly to moderately intense diffraction ring is usually associated with the stronger Debye-Scherrer arcs.

Moderately-oriented to randomly-oriented

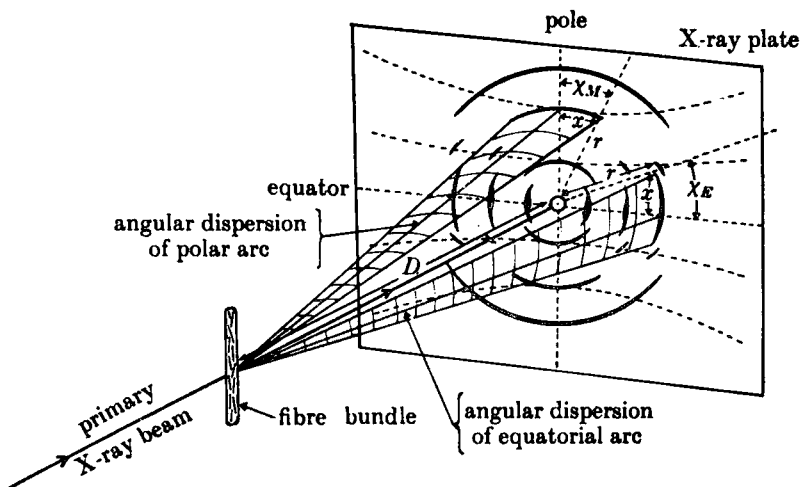


Fig. 4. The effect of disorientation of fibers, or crystals, on the shapes of the intensity maxima (from Happey 1955).

diffraction patterns have been recorded from non-fibrous, splintery to massive chrysotile  $2M_{c1}$  specimens. The moderately-oriented diffraction patterns contain Debye-Scherrer arcs of  $25^\circ$  to  $35^\circ$  which pass gradually into complete diffraction rings of weak to moderate intensity (Fig. 6c). This type of diffraction pattern grades into those with complete diffraction rings of uniform intensity around the circumference of each ring (Fig. 6e).

### Parachrysotile

Parachrysotile (Whittaker 1956c) is present occasionally as a minor component in some chrysotile  $2M_{c1}$  (Fig. 6a) and chrysotile  $2Or_{c1}$  asbestos specimens. The positions of the 020, 110 and 130 reflections indicate that the y-axis of parachrysotile lies parallel to the fiber axis.

### Lizardite

Lizardite occurs most commonly as the  $1T$

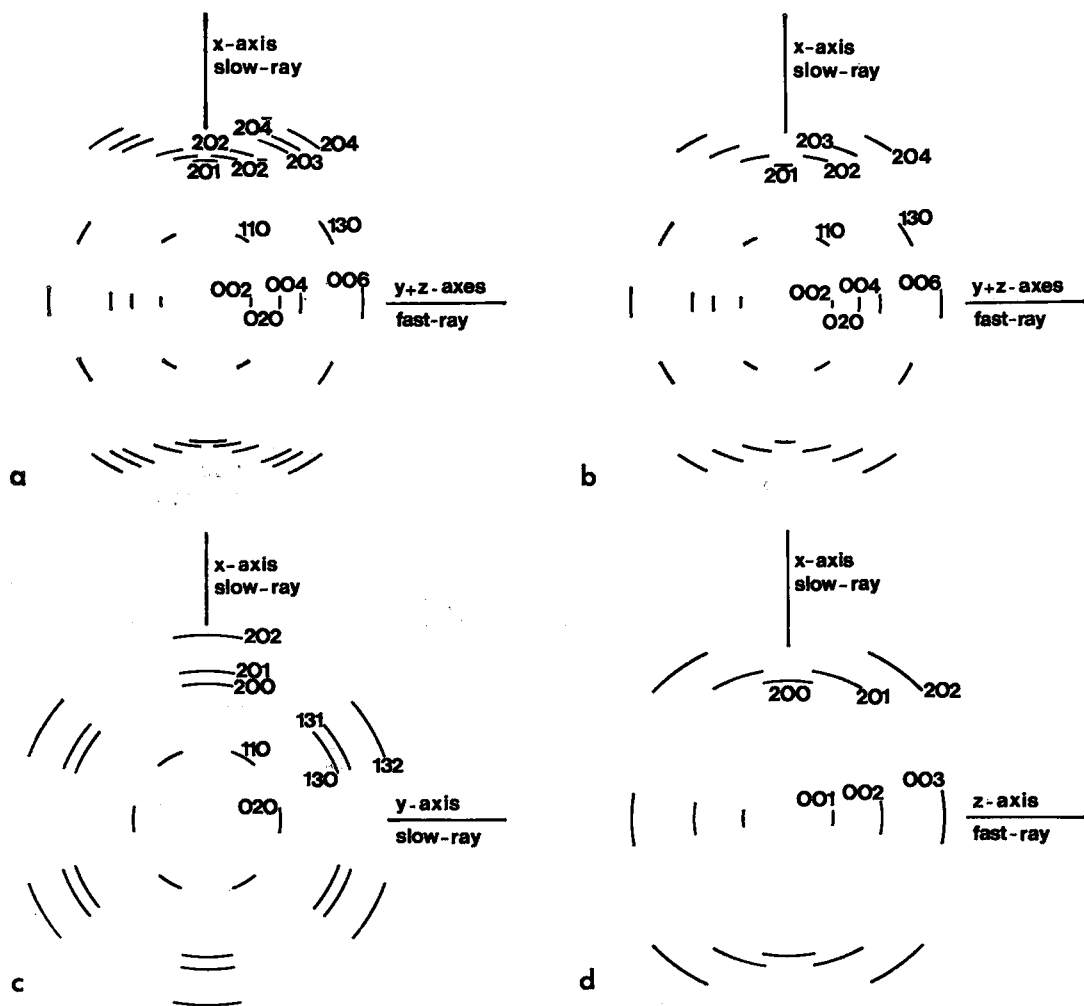


FIG. 5. Diagrammatic representations of x-ray microbeam diffraction patterns. The relative intensities of the different reflections are not indicated and the Debye-Scherrer rings often present have been omitted. The chrysotiles are indexed on the basis of a 2-layer unit cell, the lizardites and antigorite on the basis of 1-layer unit cells.

- 5a. Chrysotile  $2M_{c1}$ , x-axis vertical and normal to the microbeam.  
 5b. Chrysotile  $2Or_{c1}$ , x-axis vertical and normal to the microbeam.  
 5c. Lizardite  $1T$ , z-axis parallel to the microbeam.  
 5d. Lizardite  $1T$ , y-axis parallel to the microbeam.

polytype (Wicks & Whittaker 1975, and in preparation), but some 2-layer and 6-layer polytypes were found and will be discussed also. Except where specified otherwise, the term lizardite alone is used to denote the 1T polytype. Obvious single crystals were encountered occasionally in the course of the microbeam camera study, but most of the material, in the various textures, appeared to be composed of fine grains or apparent fibers with varying degrees of parallel orientation.

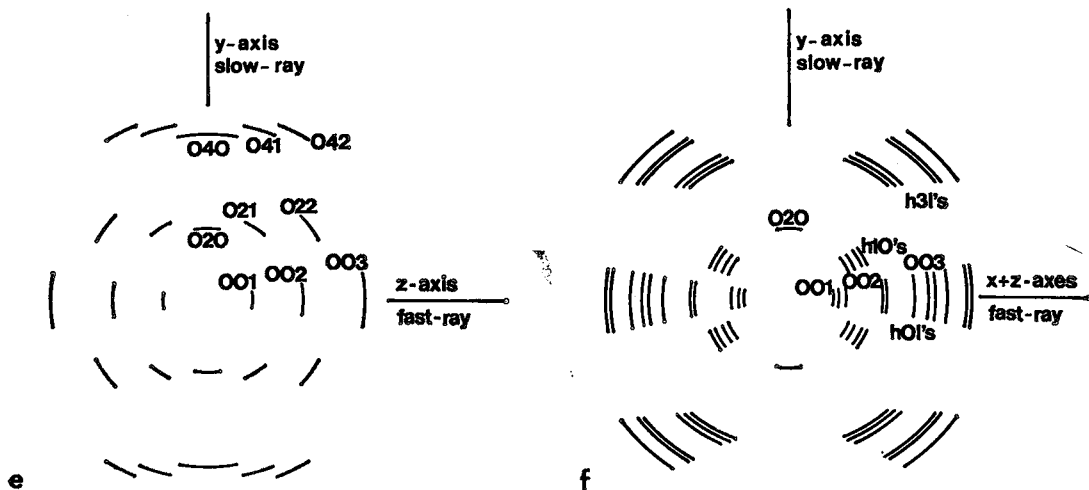
The microbeam x-ray diffraction patterns of lizardite in serpentine textures only very generally resemble normal oscillation, or rotation photographs of lizardite single crystals. The variable morphology and orientation of lizardite produces complications in the diffraction patterns that make their analyses more complex than single-crystal diffraction patterns. However, all patterns can be interpreted in terms of three somewhat idealized patterns, one with the z-axis parallel to the x-ray microbeam (Fig. 5c), one with the y-axis parallel to the x-ray microbeam (Fig. 5d), and one with the x-axis parallel to the x-ray microbeam (Fig. 5e).

When the z-axis of lizardite is parallel to the x-ray microbeam a typical hexagonal array of  $h00$ ,  $h0l$ ,  $0k0$ ,  $0kl$ ,  $hk0$  and  $hkl$  reflections is produced (Fig. 5c). The pattern produced when y is parallel to the beam is composed of  $00l$  reflections on the zero-layer line, and  $20l$  reflections on the second-layer line (Fig. 5d). When the x-axis is parallel to the beam,  $00l$  reflections again occur on the zero-layer line and  $02l$  and  $04l$  reflections occur on the second- and fourth-layer lines (Fig. 5e).

Lizardite most commonly occurs in mesh and hourglass textures after olivine, so the diffraction patterns produced from the lizardite in these textures will be discussed first. The diffraction patterns produced by the lizardite in orthopyroxene-bastites tend to be different and they will be discussed second. A detailed description of the mineralogy of the various types of textures is contained in Wicks & Whittaker (in preparation).

When lizardite in mesh textures is x-rayed with z parallel to the microbeam, a diffraction pattern with the hexagonal array is produced (compare Fig. 5c and Fig. 6f). The reflections are in the form of Debye-Scherrer arcs and are usually associated with weak diffraction rings (Fig. 6f). The Debye-Scherrer arcs span  $25^\circ$  on the most strongly oriented diffraction pattern recorded, but arcs of  $35^\circ$  are more common.

The fact that the 020 and 201 and all their symmetry-related reflections are recorded on a single photograph (Fig. 6f), indicates that some lizardite plates must be tilted  $10^\circ$  and  $2^\circ$  respectively away from a position with the z-axis parallel to the x-ray beam. This sets a conical disorientation of the lizardite plates at a minimum of  $20^\circ$  ( $2 \times 10^\circ$ ). The 202 and 132 reflections and 200 and 130 reflections are usually present; each set requires  $15^\circ$  and  $17^\circ$  of tilting respectively, and indicates at least  $35^\circ$  of conical disorientation. The 021 and 111 reflections and 040 and 220 reflections would all be in a diffracting position with the z-axis tilted  $20^\circ$  away from the x-ray beam, and since these reflections are often absent, an upper limit of approximately  $40^\circ$  of arc is put on the conical



5e. Lizardite 1T, x-axis parallel to the microbeam.

5f. Antigorite, y-axis vertical and normal to the microbeam.

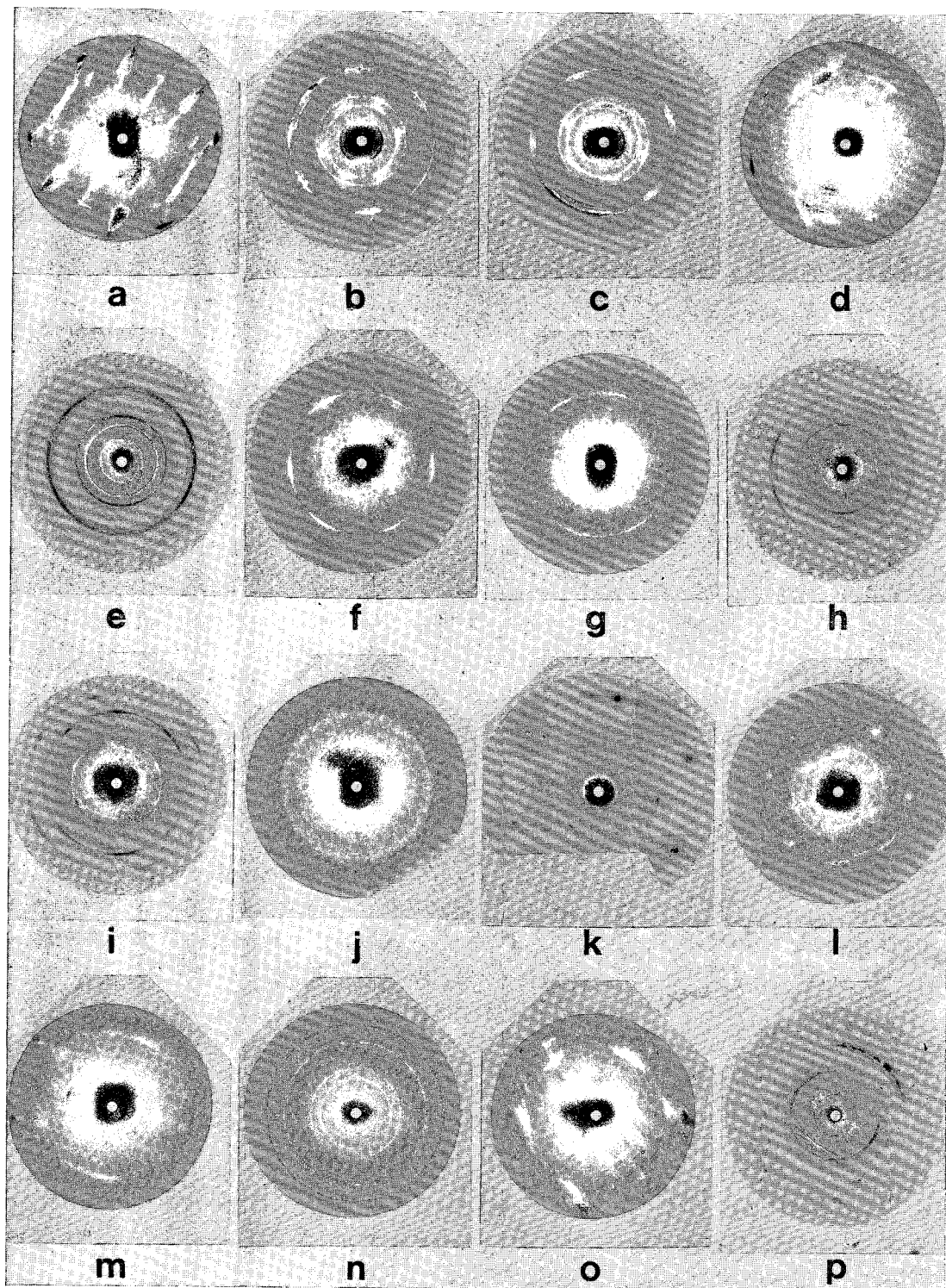


FIG. 6. X-ray microbeam diffraction patterns. Actual size.

6a. Chrysotile  $2M_{c1}$  and minor parachrysotile.

disorientation. It appears therefore, that  $35^\circ$  of conical disorientation is present in these lizardites.

When lizardite in mesh textures is  $x$ -rayed with the  $z$ -axis normal to the  $x$ -ray microbeam, a diffraction pattern composed of a series of  $00l$  reflections on the zero-layer line,  $0kl$  reflections relating to the second- and fourth-layer lines on the  $y$ -axis, and  $20l$  reflections relating to the second-layer line on the  $x$ -axis is produced (Fig. 6g). This is a combination of two diffraction patterns, one with  $y$  parallel and one with  $x$  parallel to the  $x$ -ray microbeam. (Compare Figs. 5d and 5e to Fig. 6g).

Most of the reflections occur in the form of Debye-Scherrer arcs. The stronger reflections such as 001, 002, 020, 201 and 202 are associated with complete, though often weak, Debye-Scherrer diffraction rings (Fig. 6g). The intensity usually drops rapidly in passing from the intense arc to the weak ring. Measurements on the intense 002 reflections (equivalent to 004 of chrysotile), commonly lie between  $35^\circ$  and  $40^\circ$  of arc. The recording of the  $00l$  reflections out to 003 requires that the  $z$ -axis be tilted up to  $18^\circ$  out of the plane normal to the  $x$ -ray beam, suggesting at least  $36^\circ$  of conical disorientation about the average  $z$ -axis position, a value similar to that observed above.

This conical disorientation offers an explanation as to why both  $x$ -axis and  $y$ -axis layer lines can be present on a single diffraction pattern. Because of the pseudotrigonal symmetry of lizardite any given  $x$ -axis is only  $60^\circ$  away from an alternate  $x$ -axis and only  $30^\circ$  from a  $y$ -axis (see Fig. 6f). Thus a conical disorientation of over  $30^\circ$  is enough to put some  $0kl$  and  $20l$

planes into the correct positions for diffraction (Fig. 6g). Occasionally the conical disorientation is less than  $30^\circ$  and a strong tilting effect of the  $x$ - and  $y$ -axes is produced with some  $0kl$  reflections restricted to one side of the diffraction pattern and some  $20l$  reflection restricted to the opposite side (Fig. 6h).

Figure 6i illustrates an unusually complex diffraction pattern with two set of intensity maxima.

The oriented diffraction patterns grade into randomly-oriented diffraction patterns in which the intensity is evenly distributed around the complete diffraction ring (Fig. 6j lizardite and Fig. 6e lizardite 1T with chrysotile  $2M_{c1}$ ).

In contrast to the conical disorientation of the lizardite in mesh textures, the lizardite in orthopyroxene-bastites tends to be fairly strongly oriented parallel to, or around certain crystallographic axes. The reflections tend to be in the form of sharp diffraction spots (Fig. 6k) or in Debye-Scherrer arcs up to approximately  $30^\circ$  (Fig. 6l). Conical disorientation is, therefore, either not present, or if present, is more limited than in the lizardite in mesh textures.

The diffraction patterns recorded from lizardite in orthopyroxene-bastites correspond to various combinations of the three idealized patterns (Figs. 5c, 5d, 5e). A strong hexagonal symmetry is often present in some diffraction patterns (Fig. 6k), suggesting an orientation with  $z$  parallel to the  $x$ -ray microbeam (Fig. 5c). The fact that the 201 and the 020 and all their symmetry-related reflections are recorded (Fig. 6k) indicates that some of the lizardite plates must be tilted  $2^\circ$  and  $10^\circ$  respectively away from the position with the  $z$ -axis parallel to the

- 
- 6b. Chrysotile  $2M_{c1}$  and chrysotile  $2Or_{c1}$  (Povlen-type, Middleton 1974), with  $x$ -axis slightly inclined to the microbeam.
  - 6c. Chrysotile  $2M_{c1}$  and very minor lizardite moderately well-oriented with  $x$ -axis slightly inclined to the microbeam.
  - 6d. Chrysotile  $2M_{c1}$  with  $x$ -axis strongly inclined to the microbeam.
  - 6e. Chrysotile  $2M_{c1}$  and lizardite 1T with random orientation.
  - 6f. Lizardite with  $z$ -axis parallel to the microbeam. (Note that the 101 reflections of brucite are present just outside the 201 lizardite reflections).
  - 6g. Lizardite in mesh texture with  $z$ -axis normal to the microbeam.
  - 6h. Lizardite in mesh texture with  $x$ - and  $y$ -axes inclined to the microbeam.
  - 6i. Lizardite in mesh texture with two main orientations.
  - 6j. Lizardite in mesh texture with random orientation.
  - 6k. Lizardite in orthopyroxene-bastite with  $z$ -axis parallel to microbeam.
  - 6l. Lizardite in orthopyroxene-bastite with  $y$ -axis parallel to, and  $x$ -axis slightly inclined to, the microbeam.
  - 6m. Lizardite with orthopyroxene-bastite with  $y$ - and  $z$ -axes inclined to the microbeam.
  - 6n. Lizardite (6-layer) with near-random orientation.
  - 6o. Antigorite with  $y$ -axis normal to the microbeam.
  - 6p. Antigorite with  $y$ -axis inclined to the microbeam.

x-ray beam. The 202 and symmetry-related reflections require  $15^\circ$  of tilting and are present when the reflections show some conical disorientation, but are absent when reflections are in the form of sharp diffraction spots (Fig. 6k).

The 130 set of reflections requires  $17^\circ$  of tilting and similarly may or may not be present. The 200 and  $\bar{2}00$  reflections, which also require  $17^\circ$  of tilting, are usually absent, suggesting that the alignment of lizardite plates is fairly rigorously parallel to  $x$  but is much less rigorously oriented around the  $x$ -axis. This is further supported by the presence of 00 $l$  reflections indicating that some of the lizardite is oriented with  $z$  at a high angle to the  $x$ -ray microbeam. Thus Figure 6k is composed of the diffraction pattern in Figure 5d superimposed on the pattern in Figure 5c. This explains the three 201 reflections at the top of Figure 6k. The central one is produced by lizardite with  $z$  parallel to the beam and the flanking pair is produced by lizardite with  $y$  parallel to the beam (compare Fig. 6k and Figs. 5c and 5d).

A further complicating factor is the presence of weak 020 reflections lying between the pairs of 110 reflections and at  $90^\circ$  to the 020 reflections produced by lizardite with  $z$  parallel to the  $x$ -ray microbeam (Fig. 6k). These 020 reflections, when they are fairly intense, are associated with 021- and 022-series reflections (Fig. 6l) and indicate that some of the lizardite is oriented with  $x$  parallel to the  $x$ -ray microbeam (Fig. 5e). Thus in a single diffraction pattern three orientations of lizardite are indicated (Figs. 5c, 5d and 5e superimposed). Many of the reflections lie on weak, incomplete or complete Debye-Scherrer rings. The diffraction rings indicate a certain amount of random orientation.

A complete gradation from the diffraction pattern described above (Fig. 6k) in which the dominant pattern is  $z$ -axis parallel to the beam (Fig. 5c) to a pattern in which the dominant pattern is  $y$ -axis parallel to the beam (Fig. 5d) has been recorded (Fig. 6l). Again this latter pattern is a combination of all three patterns but the  $y$ -axis parallel to the beam dominates. The 1 $kl$  series of reflections are weaker than in Figure 6k and the 020 reflections are absent or very weak. The 20 $l$  reflections are more intense and occur as slightly broader arcs than the equivalent 13 $l$  reflections. The broadness is due to their proximity to the line of the  $x$ -axis which has the same effect as a rotation axis. The 20 $l$  and equivalent 13 $l$  reflections usually are joined by very weak continuous or discontinuous diffraction rings. The 200 reflections are usually absent although weak 130 reflections are very often present.

Lizardite in an intermediate position with neither the  $z$ - or  $y$ -axis dominantly parallel to the  $x$ -ray beam produces diffraction patterns with marked differences in intensity between equivalent reflections across the plane of the  $x$ -axis (Fig. 6m). This is particularly noticeable between pairs of 00 $l$ , 1 $kl$  and 20 $l$  reflections. An 020 reflection may be present on one side of the diffraction pattern and absent on the other (Fig. 6m). This asymmetry of intensities indicates that completely random orientation is not developed about the  $x$ -axis.

The final possible variation in the diffraction pattern from lizardite in orthopyroxene-bastites is a combination of the diffraction pattern with  $y$  parallel to the beam (Fig. 5d) and the diffraction pattern with  $x$  parallel to the beam (Fig. 5e). It is composed of strong pairs of 001 and 002 reflections with or without a pair of 003 reflections on the zero-layer line, 020 reflection on the second-layer line with respect to the  $y$ -axis and a strong series of 20 $l$  reflections on the second-layer line relating to the  $x$ -axis. The 110 and 13 $l$  series of reflections are absent. This is essentially the same as the diffraction pattern from lizardite in mesh textures (Fig. 6g) except that the Debye-Scherrer arcs are shorter,  $35^\circ$  or less, indicating that the conical distortion is less.

The diffraction patterns from lizardite in orthopyroxene-bastites indicate that although any given area will contain lizardite in three orientations, disorientation about these positions is not completely random but is limited to within approximately  $30^\circ$  from the ideal. The orientation parallel to the  $x$ -axis is even more closely limited.

Occasionally in some diffraction patterns from lizardite in both mesh textures and orthopyroxene-bastites, weak reflections were recorded between the 201 and 202 reflections. These reflections cannot be indexed using a 1-layer cell, but can be indexed as 203 reflections of a 2-layer cell, suggesting that minor amounts of a 2-layer lizardite are intimately associated with the 1-layer lizardite.

Lizardites with 6-layer structures have also been encountered. They produce diffraction patterns with spotty, but complete Debye-Scherrer rings (Fig. 6n). Usually the diffraction pattern shows little preferred orientation.

### *Antigorite*

The microbeam diffraction pattern of antigorite in general resembles a normal fiber diffraction pattern of splintery antigorite. A diagrammatic representation of the antigorite microbeam diffraction pattern is given in Figure

5f. The  $y$ -axis is parallel to the blade or splinter axis of antigorite. The zero-layer line contains both  $00l$  and  $h0l$  reflections because the  $z$ - and  $x$ -axes lie randomly or semi-randomly about the  $y$ -axis position. The first- and third-layer lines contain  $h1l$  and  $h3l$  reflections respectively. The second layer line is composed of the  $020$  reflection only. Because of the superlattice along the  $x$ -axis, the diffraction pattern of antigorite contains more reflections than the diffraction patterns of most of the other serpentine minerals.

The reflections on antigorite microbeam diffraction patterns occur as sharp diffraction spots, not smooth Debye-Scherrer arcs (Figs. 6o and 6p). On moderately to well-oriented diffraction patterns the diffraction spots of the stronger reflections, such as the  $00l$  reflections, overlap to form spotty  $20^\circ$  to  $50^\circ$  arcs, but in the weaker reflections individual diffraction spots can usually be distinguished (Fig. 6p). A peculiar, characteristic streaking is present also (Fig. 6o). The origin of this streaking is not well-understood, but may possibly be due to variations in the superlattice or some other form of disorder. The less strongly oriented and randomly oriented microbeam diffraction patterns of antigorite also contain streaking and sharp diffraction spots.

The antigorite microbeam diffraction pattern could be explained in terms of "end-member" diffraction patterns, similarly to the way the lizardite patterns were described. However, for simplicity this procedure has not been followed. In practice it appears that groups of parallel or sub-parallel antigorite blades are always included within the 50 micron beam diameter and their semi-random orientation about the  $y$ -axis produces near "rotation-type" photographs. Also, the characteristic streaking associated with the antigorite reflections tends to mask the fine details of the microbeam diffraction patterns (Fig. 6o). In spite of this, differences in intensity between equivalent reflections across the line of the  $y$ -axis are observed, and suggest that the orientation of antigorite about the  $y$ -axis is not completely random.

Tilting of the  $y$ -axis towards the top of the film draws together the pairs of  $hkl$  reflections and weakens the  $020$  reflection on the top half of the film, and spreads apart the pairs of  $hkl$  reflections and intensifies the  $020$  reflection on the bottom half (Fig. 6p).

#### CRYSTAL MORPHOLOGY AND OPTICAL CLASSIFICATION

When examined in thin section, many of the

textural units appear to be composed of fibrous serpentine. A detailed classification of serpentine mineral textures and the results of microbeam  $x$ -ray camera studies of these textures is the subject of another paper (Wicks & Whittaker, in preparation). An optical classification has been developed (Tertsch 1922) based on the elongation of the apparent fibers. Apparent fibers with negative elongation (length-fast) are called  $\alpha$ -serpentine and apparent fibers with positive elongation (length-slow) are called  $\gamma$ -serpentine.

The lizardite that makes up the mesh rims and hourglass textures, formed after olivine, (and certain serpentine pseudomorphs after pyroxenes and amphiboles) usually appears as apparently fibrous  $\alpha$ -serpentine. The apparent fibers lie at right angles to the mesh rim walls in coincidence with the fast-ray ( $\alpha$ -ray) and the  $z$ -axis of the lizardite (Figs. 5d, e). Although this lizardite or  $\alpha$ -serpentine appears to be composed of fibers, the microbeam  $x$ -ray diffraction patterns contain some features that resemble single-crystal patterns. The strong hexagonal pattern produced when the lizardite  $z$ -axis, the apparent fiber-axis, is parallel to the microbeam (Fig. 5c) indicates that there is a strong crystallographic continuity, within  $30^\circ$  to  $40^\circ$  of arc, between the adjacent apparent fibers. This continuity is not restricted to the 50 micron diameter area exposed to the microbeam, but is continuous across a given textural unit. Thus the apparent fibers of  $\alpha$ -serpentine do not appear to be fibrous in the same sense that chrysotile asbestos is fibrous. However, the spread of the reflections into  $30^\circ$  to  $40^\circ$  arcs indicates that the  $\alpha$ -serpentine textural units are not ordinary well-formed crystals either.

There are various interpretations. The  $\alpha$ -serpentine apparent fibers may be individual "fibers" each made up of piles of lizardite platelets stacked with  $z$ -axes in coincidence and lying along the fiber axis. The "fibers" may be parallel, and within each "fiber" the platelets may be conically distorted over  $30^\circ$  to  $40^\circ$  of arc, or the platelets may be undistorted and planar within each "fiber" and the "fibers" conically disoriented with respect to each other within  $30^\circ$  to  $40^\circ$  of arc. In each case the "fibers" must be crystallographically related to each other within the  $30^\circ$  to  $40^\circ$  of arc. However, observations on finely ground and dispersed samples of this material with both petrographic and transmission electron microscopes reveal only angular, equant fragments and no elongate fibers. An alternative interpretation is that each  $\alpha$ -serpentine textural unit is a large imperfect or distorted single crystal or

several large single crystals that produce the arc-shaped reflections, and an apparently fibrous appearance when sectioned.

The lizardite pseudomorphs after orthopyroxene-bastites are composed of apparently fibrous  $\gamma$ -serpentine. The apparent fibers lie parallel to the original orthopyroxene cleavage in coincidence with the slow-ray ( $\gamma$ -ray) and the  $x$ -axis of lizardite (Figs. 5c, d).

The microbeam diffraction patterns of chrysotile asbestos fibers are essentially similar to normal-fiber diffraction patterns. The fiber axis, the slow-ray ( $\gamma$ -ray) and the  $x$ -axis of chrysotile are parallel (Figs. 5a, b) so that chrysotile is one form of  $\gamma$ -serpentine.

There are certain similarities between the diffraction patterns of chrysotile and of lizardite in orthopyroxene-bastites (compare Fig. 6a to Figs. 6l and 6m). However, in spite of these superficial similarities, the morphology of chrysotile fibers and lizardite apparent fibers is very different. Because of the cylindrical structure of chrysotile (Whittaker 1953, 1956a, b; Yada 1967, 1971) the intensities of equivalent reflections on both sides of the line of the  $x$ -axis are equal. In lizardite diffraction patterns from orthopyroxene-bastite, the variations in intensities and the presence and absence of equivalent reflections (in particular the 020 reflections) across the line of the  $x$ -axis are incompatible with diffraction from a cylindrical structure. These suggest that the lizardite crystals take the form of elongate laths with their  $x$ -axes strongly parallel to each other but with a certain amount of, but not a total, random orientation around the  $x$ -axes. The lizardite  $\gamma$ -serpentine apparent fibers are not, therefore, fibrous in the same sense as chrysotile asbestos fibers. In previous studies (Zussman *et al.* 1957), when finely ground and dispersed lizardite from orthopyroxene-bastites were examined by electron microscopy, only irregular equant grains and no fibers were observed.

Antigorite microbeam diffraction patterns are usually recorded from sub-parallel blades, laths or apparent fibers of serpentine. The long axis of these particles, the slow-ray ( $\gamma$ -ray), and the  $y$ -axis are parallel (Fig. 5f). This is a different orientation from the orientation of chrysotile or  $\gamma$ -serpentine lizardite however. The blades are length-slow so that, optically, antigorite also can be classified as a form of  $\gamma$ -serpentine.

Antigorite microbeam diffraction patterns often have differences in equivalent reflections across the line of the  $y$ -axis, which suggest that antigorite is composed of laths with their  $y$ -axes approaching parallel orientation, but with partial disorientation around the  $y$ -axes.

The term serpophite was suggested by Lodochnikov (1933) to describe the featureless, isotropic or near-isotropic serpentine found in mesh centers of mesh textures after olivine and in some fracture-filling serpentine veins. Microbeam camera studies of serpophite in mesh centers usually produce random or nearly random lizardite diffraction patterns (Fig. 6j). Microbeam camera studies of serpophite in fracture-filling serpentine veins produce random lizardite, random chrysotile  $2M_{ca}$  or combined random lizardite and chrysotile  $2M_{ca}$  diffraction patterns (Fig. 6e).

Whether these random-diffraction patterns are recorded from mesh centers or fracture-filling veins, the diffraction rings usually are smooth and free of diffraction spots. Some of the diffraction rings are broadened (Fig. 6j) suggesting that the serpentine crystals are not only randomly oriented but are finer and/or less perfectly formed crystals than the lizardite in mesh rims, hourglass textures and bastites. Thus a combination of very fine grain size and random orientation is usually responsible for the isotropic appearance. Occasionally a hexagonally-arrayed diffraction pattern of lizardite is recorded, indicating that lizardite is being viewed down the  $z$ -axis and is isotropic for this reason (Fig. 6f).

Lizardites with 6-layer structures usually occur as  $\alpha$ -serpentine in fracture-filling veins, but unlike the isotropic serpentine, the microbeam patterns have diffraction rings composed of sharp spots (Fig. 6n). Antigorite diffraction patterns also have sharp diffraction spots (Figs. 6o, p). These sharp spots suggest that 6-layer lizardite and antigorite are coarser-grained, more perfectly crystallized, or both, than the lizardite  $1T$  occurring in mesh, hourglass textures, bastites and fracture-filling veins.

The foregoing results suggest that, of all the apparently fibrous serpentine observed in thin sections, only chrysotile asbestos is truly fibrous. The term fibrous, therefore, should be used with restraint in petrographic descriptions of serpentine minerals and qualified as apparently fibrous unless the fibrous property has been definitely established.

The microbeam diffraction results indicate that the terms  $\alpha$ -serpentine,  $\gamma$ -serpentine and serpophite have no strict mineralogical meaning.  $\alpha$ -serpentine may be lizardite in mesh or hourglass textures, or 6-layer lizardite;  $\gamma$ -serpentine may be chrysotile, lizardite in orthopyroxene-bastites, or antigorite. Serpophite may be lizardite, chrysotile or a mixture of the two. The terms  $\alpha$ - and  $\gamma$ -serpentine can be useful for petrographic descriptions prior to  $x$ -ray analysis, but if their use is to be continued they

must be petrographic terms only, with no very specific mineralogical implications.

#### THEORETICAL RELATIONSHIP BETWEEN OPTICAL PROPERTIES AND CRYSTALLOGRAPHIC AXES

Since the position of the crystallographic axes can be located with the microbeam camera and the optical properties can be determined with the petrographic microscope, it is now possible to continue the discussion begun by Francis (1956) and to explain both the optical characteristics of the serpentine minerals in relationship to one another, and the variations brought about by the orientation of the minerals within different textural units.

A discussion of the optical properties of idealized single crystals or fibers of the serpentine minerals can begin with lizardite (Fig. 7). The idealized lizardite structure is planar and trigonal, but the optical properties are given in terms of an orthohexagonal cell (for ease of comparison with chrysotile and antigorite) as  $\alpha$  vibrating parallel to the  $z$ -axis,  $\beta$  vibrating parallel to the  $x$ -axis and  $\gamma$  vibrating parallel to the  $y$ -axis (Fig. 7). The published refractive indices range from  $\alpha = 1.538 - 1.562$ ,  $\beta = \gamma = 1.546 - 1.570$  (Wicks 1969, p. 147). These are the figures of Deer, Howie & Zussman (1962) revised to include the results of Nagy & Faust (1956), Chidester (1962), Peters (1963), and Page & Coleman (1967).

The idealized structure of chrysotile can be formed by wrapping the idealized lizardite sheets about the  $x$ -axis to form a spiral or concentric structure (Fig. 7). The curving will have the

least effect on the refractive index parallel to the  $x$ -axis, the axis of curvature, but will produce a refractive index at right angles to the axis of curvature that contains elements of the refractive index parallel to  $z$  and the refractive index parallel to  $y$ . The net result is necessarily less than  $\beta$  for lizardite. Therefore in chrysotile the refractive index at right angles to the axis of curvature will be  $\alpha$  and the refractive index parallel to the axis of curvature will be  $\gamma$ . The published refractive indices of chrysotile range from  $\alpha = 1.532 - 1.569$  and  $\gamma = 1.540 - 1.570$  (Wicks, 1969, p. 147).

Parachrysotile is curved about the  $y$ -axis (Fig. 7) so that  $\gamma$ , the refractive index parallel to the  $y$ -axis, will lie along the fiber axis; however, since  $\gamma = \beta$  in lizardite, the optical properties of parachrysotile will be the same as chrysotile so that parachrysotile will also be length-slow. Because of the cylindrical structure, fibers of chrysotile and parachrysotile will be isotropic when viewed down the fiber axis.

The relationship of the refractive indices and the crystal axes found for antigorite by Zussman (1954) and Francis (1956) was  $\alpha$  vibrating approximately parallel to  $z$ ,  $\beta$  vibrating approximately parallel to  $x$ , and  $\gamma$  vibrating approximately parallel to  $y$  (Fig. 7). This relationship can now be explained in terms of an ideal lizardite structure. In lizardite,  $\beta = \gamma$ , but antigorite differs from lizardite because its structure is in the form of alternating waves curved about the  $y$ -axis and propagated along the  $x$ -axis. This change in the structure changes the optical properties so that the refractive index parallel to  $x$  is lower than that parallel to  $y$ ; thus  $\beta$  no

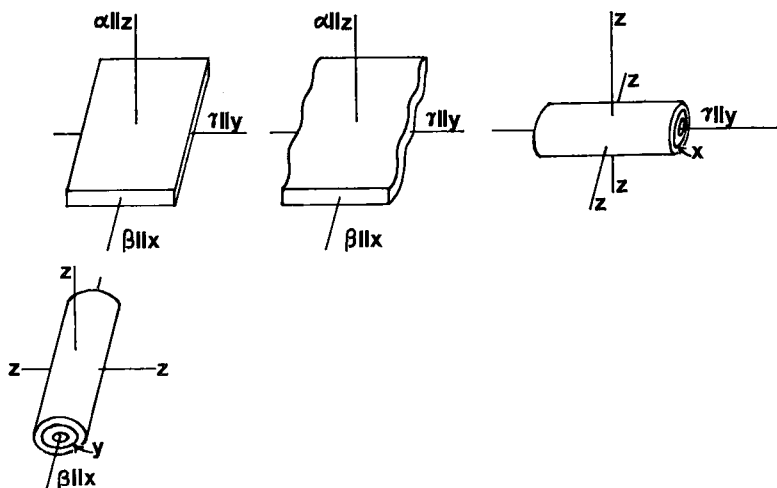


FIG. 7. A diagrammatic representation of the optical relationships among lizardite, chrysotile, parachrysotile and antigorite.

longer equals  $\gamma$ . The published refractive indices of antigorite range from  $\alpha = 1.556 - 1.573$ ,  $\beta = 1.560 - 1.577$ ,  $\gamma = 1.562 - 1.578$  (Wicks 1969, p. 147).

#### OBSERVED OPTICAL PROPERTIES IN SERPENTINE TEXTURES

When the serpentine minerals occur in the various textures their optical properties are slightly modified from idealized single crystals. This occurs because the serpentine in the textures is not in the form of single crystals, but in the form of laths, apparent fibers, or grains with varying degrees of parallel orientation, and because some of the serpentine grains may themselves be conically distorted.

The lizardite 1T that occurs in mesh and hourglass textures (Figs. 5d, e) appears as sub-parallel length-fast apparent fibers in thin section. The microbeam camera study indicates that the z-axis is sub-parallel to the apparent fiber-axis. Thus, when the elongation of the apparent fibers is determined, some value near  $\alpha$ , which is parallel to the z-axis (Fig. 7), is compared with some value near  $\gamma$ , so that the apparent fibers are length-fast (negative elongation). When the same apparent fibers of lizardite are viewed down the z-axis (Fig. 5c)  $\beta$  is compared to  $\gamma$  and since  $\beta = \gamma$  the lizardite appears to be isotropic in this position (Fig. 7).

Lizardites with 2-layer and 6-layer structures are similar to lizardite 1T.

The lizardite 1T that occurs in bastites after orthopyroxenes (Figs. 5c, d) appears as sub-parallel, length-slow laths or apparent fibers in thin section. The microbeam camera study indicates that the x-axis is sub-parallel to the lath axis and that the z- and y-axes of associated laths are crudely oriented at right angles to each other. When the elongation of these laths is determined,  $\beta$  is compared with a refractive index intermediate to  $\alpha$  and  $\gamma$  (Fig. 7). As there is always a certain amount of disorientation of the z- and y-axes about the x-axis,  $\beta$  is never compared to either  $\alpha$  or  $\gamma$  directly, but since  $\beta$  is greater than  $\alpha$  or any combination of  $\alpha$  and  $\gamma$ , the laths will be length-slow (positive elongation). When a specimen is viewed directly down the x-axis some value near  $\alpha$  will be compared to some value near  $\gamma$  so that this lizardite will never be isotropic.

Antigorite often occurs in interpenetrating textures as sub-parallel blades which are length-slow with the y-axis lying along the blade axis (Fig. 5f) and the z- and x-axes in associated blades randomly or partly oriented with respect to each other. Thus when the elongation

of the blades is determined,  $\gamma$  vibrating parallel to the y-axis is compared with  $\alpha$  or  $\beta$  or some value intermediate to  $\alpha$  and  $\beta$ . As  $\gamma$  will always be greater than any combination of  $\alpha$  and  $\beta$ , the blades will always be length-slow (Fig. 7).

When blades partly oriented about the y-axis are viewed down the y-axis, the situation is similar to lizardite laths in orthopyroxene-bastites viewed down the x-axis. In antigorite, some value near  $\alpha$  will be compared with some value near  $\beta$  and the blades will not appear isotropic in this view, unless the antigorite blades are very fine and are randomly oriented about the y-axis. These conditions rarely occur.

Chrysotile often occurs in interpenetrating textures and in veins as parallel or sub-parallel length-slow fibers with the x-axis parallel to the fiber axis. Parachrysotile has the y-axis parallel to the fiber axis, but it is also length-slow (Fig. 7) and optically indistinguishable from chrysotile. Since  $\gamma$  is always greater than  $\alpha$ , fibers of either chrysotile or parachrysotile will always appear to be length-slow, unless they are viewed along the fiber axis in which case they are isotropic. Some of the chrysotile asbestos in cross-fiber veins display anomalously high birefringence, up to second-order blues and greens. This is produced by the compression of the fibers during the grinding of the thin section, followed by the expansion of the fibers after grinding to a thickness greater than 0.03 mm, and is not an indication of any unusual property of the fibers.

If any of the serpentine minerals are very fine-grained and in random orientation, they will appear to be isotropic. Observations indicate that this happens most commonly in lizardite and chrysotile.

An examination of the microbeam diffraction patterns of all the serpentine minerals (Fig. 5) indicates that the fast ray always lies along the mean z-axis direction, even if there is appreciable spread of orientation, and whether or not the z-axis is the apparent fiber axis. Thus, when examining an unidentified serpentine mineral in thin section, it is always possible to determine the position of the z-axis.

#### SUMMARY AND CONCLUSIONS

Each of the serpentine minerals has its own characteristic powder pattern, but the microbeam diffraction pattern varies according to orientation of the sample with respect to the x-ray beam, and the orientation of the serpentine crystallites or fibers with respect to each other. However, each variety of microbeam diffraction pattern is distinct and recognizable.

The diffraction patterns of chrysotile and par-chrysotile display the effect of tilting of the fiber axis towards the  $x$ -ray microbeam and/or the effect of random or parallel orientation.

The layer structure of lizardite produces more-varied microbeam diffraction patterns, depending on the relationship of the crystallographic axes to the  $x$ -ray microbeam. The lizardite 1T platelets in mesh and hourglass textures display a conical disorientation of about 35°. The lizardite 1T in orthopyroxene-bastites has  $x$  in adjacent laths fairly strictly oriented with a maximum variation of less than 30°. The  $z$ - and  $y$ -axes are very roughly oriented at 90° to each other. Lizardites with 6-layer structures tend to produce spotty reflections, in contrast to the smooth diffraction arcs from lizardite 1T.

The diffraction patterns of antigorite also contain spotty reflections with a characteristic streaking. Variations in the diffraction patterns of antigorite are less obvious than in lizardite, as there is generally less parallel orientation between adjacent antigorite crystallites than between adjacent lizardite crystallites.

Although the serpentine in many of the textural units observed in thin section appears to be fibrous, the microbeam  $x$ -ray diffraction results suggest that only chrysotile asbestos is truly fibrous. Lizardite appears to form either plates or laths, and antigorite forms plates, blades, or laths, rather than true fibers. In petrographic descriptions the term "apparently fibrous serpentine" should be used unless the fibrous nature of the serpentine can be proven.

Antigorite and 6-layer lizardite form coarser and/or more perfect crystals than most lizardite 1T or chrysotile.

It has been shown that the terms " $\alpha$ -serpentine", " $\gamma$ -serpentine" and "serpophite" have no trict mineralogical meaning, and should be used only as petrographic terms.  $\gamma$ -serpentine may be chrysotile, lizardite, or antigorite;  $\alpha$ -serpentine is normally lizardite, and serpophite may be lizardite or chrysotile, or a mixture of the two. Regardless of the optical classification of the serpentine the fast ray always marks the position of the  $z$ -axis.

#### ACKNOWLEDGMENTS

The authors wish to thank Dr. E. J. W. Whitaker, Reader in Mineralogy, Oxford, for his advice and help during part of the research and Drs. J. A. Mandarino and R. I. Gait, Royal Ontario Museum, Toronto, for their comments on the manuscript. The permission to publish Figs. 3 and 4 by John Wiley and Sons, Inc., New York, and Associated Book Publishers Ltd.,

London, respectively, is gratefully acknowledged. Thanks is also extended to Mr. J. Mulock, ROM Art Department, who drafted Figs. 5 and 7, and the ROM Photography Department who took all the photographs.

One of us (F.J.W.) wishes to thank the Institute of Mining and Metallurgy, London, for granting him the Edgar Pam Fellowship for the academic year 1966-67 when much of this research was carried out. The Fellowship was established by the late Mrs. Millicent Pam in 1966 in memory of her husband, Lieutenant-Colonel Edgar Pam. Mrs. Pam took a keen interest in the progress of this work, which was much appreciated by the recipient.

#### REFERENCES

- BERGMANN, M. E. (1959):  $X$ -ray micro-diffraction cameras. *Norelco Reporter* 6, 96-100.
- CARRIGY, M. A. & MELLON, G. B. (1964): Authigenic clay mineral cements in Cretaceous and Tertiary sandstones of Alberta. *J. Sed. Petrol.* 34, 461-472.
- & POTHECARY, D. B. (1964):  $X$ -ray diffraction microcamera technique for identification of clay minerals in sandstones. *Norelco Reporter* 11, 138-139.
- CHESLEY, G. F. (1947):  $X$ -ray diffraction camera for micro-techniques. *Rev. Sci. Instr.* 18, 422-424.
- CHIDESTER, A. H. (1962): Petrology and geochemistry of selected talc-bearing ultramafic rocks and adjacent country rocks in north-central Vermont. *U.S. Geol. Surv. Prof. Paper* 345, 1-207.
- DEER, W. A., HOWIE, R. A. & ZUSSMAN, J. (1962): *Rock-Forming Minerals* 3. Sheet Silicates. Longmans, London.
- FRANCIS, G. H. (1956): The serpentinite mass in Glen Urquhart, Inverness-shire, Scotland. *Amer. J. Sci.* 254, 201-226.
- HAPPEY, F. (1955): Preferred orientation in organic polycrystalline materials. In *X-ray Diffraction by Polycrystalline Materials*. Peisser, H. S., Rooksby, H. P. & Wilson, A. J. C. eds. Inst. Physics, London.
- KLUG, H. P. & ALEXANDER, L. E. (1954): *X-ray Diffraction Procedures*. John Wiley & Sons Inc., New York.
- LODOCHNIKOV, W. N. (1933): Serpentes and serpentinites and the petrological problems connected with them. *Problems Soviet Geol.* 2, 145-150.
- MIDDLETON, A. P. (1974): *Crystallographic and Mineralogical Aspects of Serpentine*. D.Phil. thesis, Oxford Univ., Oxford, England.
- NAGY, B. & FAUST, G. T. (1956): Serpentes: natural mixtures of chrysotile and antigorite. *Amer. Mineral.* 41, 817-838.
- PAGE, N.J. & COLEMAN, R. G. (1967): Serpentine-mineral analyses and physical properties. *U.S. Geol. Surv. Prof. Paper* 575B, 103-107.

- PETERS, T.J. (1963): Mineralogie und Petrographie des Totalserpentins bei Davos. *Schweiz. Mineral. Petrogr. Mitt.* **43**, 529-685.
- TERTSCH, H. (1922): Studien am Westrande des Dunkelsteiner Granulitmassivs. *Tschermaks Mineral. Petrogr. Mitt.* **35**, 177-214.
- WHITTAKER, E. J. W. (1953): The structure of chrysotile. *Acta Cryst.* **6**, 747-748.
- (1956a): The structure of chrysotile. II. Clinochrysotile. *Acta Cryst.* **9**, 855-862.
- (1956b): The structure of chrysotile. III. Orthochrysotile. *Acta Cryst.* **9**, 862-864.
- (1956c): The structure of chrysotile. IV. Parachrysotile. *Acta Cryst.* **9**, 865-867.
- & ZUSSMAN, J. (1956): The characterization of serpentine minerals by x-ray diffraction. *Mineral. Mag.* **31**, 107-126.
- WICKS, F. J. (1969): *X-ray and Optical Studies on Serpentine Minerals*. D.Phil. thesis, Oxford Univ., Oxford, England.
- & WHITTAKER, E. J. W. (1975): A reappraisal of the structures of the serpentine minerals. (this issue).
- & ——— (in preparation): Serpentine textures and serpentinization.
- YADA, K. (1967): Study of chrysotile asbestos by a high resolution electron microscope. *Acta Cryst.* **23**, 704-707.
- (1971): Study of microstructure of chrysotile asbestos by high resolution electron microscopy. *Acta Cryst.* **A27**, 659-664.
- ZUSSMAN, J. (1954): Investigation of the crystal structure of antigorite. *Mineral. Mag.* **30**, 498-512.
- , BRINDLEY, G. W. & COMER, J. J. (1957): Electron diffraction studies of serpentine minerals. *Amer. Mineral.* **42**, 133-153.
- ZVYAGIN, B. B. (1967): *Electron-Diffraction Analysis of Clay Mineral Structures*. R. W. Fairbridge, ed., Plenum Press, N.Y.

*Manuscript received January 1975.*